View metadata, citation and similar papers at core.ac.uk
brought to you by CORE
provided by CONICET Digital

# MODELING MELT SPINNING WITH STRESS INDUCED CRYSTALLIZATION AT HIGH TAKE UP VELOCITIES. NUMERICAL RESULTS FOR THE PET MELT

**Mariel L. Ottone, Marta B. Peirotti and Julio A. Deiber**

Instituto de Desarrollo Tecnológico para la Industria Química
(INTEC-UNL-CONICET)
Güemes 3450, 3000 Santa Fe, Argentina
e-mail: treoflu@ceride.gov.ar

**Key words**: Melt spinning, stress induced crystallization, filament necking, polyethylene therephtalate filament, high take up velocity.

**Abstract.** *The purpose of this work is to present a 2D thermo-rheological model for high take up velocities that can predict numerically in the filament domain, the axial velocity profile together with the radial and axial resolutions of stresses, temperature and degree of crystallization. The rheology of the filament is described through a constitutive equation that results from the combination of the Phan-Thien and Tanner viscoelastic model for the amorphous phase and the kinetic model of the rigid dumbbell for the crystalline phase immersed in the melt. The model is thus able to predict the thermal and mechanical coupling between both phases through the degree of transformation (relative degree of crystallization) when the balances of mass, momentum and energy are invoked. The effects of stress induced crystallization, viscoelasticity, friction of cooling air, filament inertia, gravity and surface tension are all considered together with the temperature dependency of polymer and cooling air thermo-physical properties. The rate of crystallization is evaluated through the non-isothermal Avrami-Nakamura equation. Also, the relaxation times of both phases are function of temperature and degree of transformation. Numerical predictions of the model compare well with experimental data reported in the literature for a PET melt at a take up velocity of 5490 m/min. Also, consistently with experimental observations reported in the literature, the "skin-core" structure is predicted. It is relevant to indicate that the model analyzed here can be evaluated from low to high take up velocities, and when the degree of crystallization becomes negligible, the one-phase model is recovered continuously.*

## 1 INTRODUCTION

The conventional melt spinning operation for synthetic polymers is carried out at relatively low take up velocities (less than 3500 m/min). Therefore, the fiber thus obtained requires further mechanical (cold drawing) and thermal (heat annealing) treatments to achieve the final properties required for commercial uses. At present, high take up velocities are being used in the spinneret to reduce these treatments, and also to improve certain fiber mechanical responses. Nevertheless, to be successful in this sense, several physical aspects and challenging basic problems must be still considered and solved in the production of fibers; for instance, appropriate quantification of physical aspects like molecular orientation of the amorphous phase due to the elongational flow imposed, non-isothermal crystallization induced by stresses, changes in the polymer rheological properties due to the evolutions of the amorphous and crystalline phases, among other relevant phenomena associated to this complex operation of the polymer processing.

One of the consequences of the high values of take up velocity required (typically higher than 4500 m/min) is the neck formation (sudden reduction of filament radius) at a given position of the filament (Figure 1), where stress induced crystallization mainly occurs. Therefore, in this context of analysis, the purpose of this work is to present a 2-D thermo-rheological model for high take up velocities that can predict, in the filament domain, the axial velocity profile together with the radial and axial resolutions of stresses, temperature and degree of crystallization. The rheology of the filament is described through a constitutive equation that results from the combination of the Phan-Thien and Tanner viscoelastic model for the amorphous phase and the kinetic model of the rigid dumbbell for the crystalline phase immersed in the melt, by following in part the previous works of Doufas et al.[1] The model is thus able to predict the thermal and mechanical coupling between both phases through the degree of transformation (relative degree of crystallization) when the balances of mass, momentum and energy are invoked. The effects of stress induced crystallization, viscoelasticity, friction of cooling air, filament inertia, gravity and surface tension are all considered together with the temperature dependency of polymer thermo-physical properties. The rate of crystallization is evaluated through the non-isothermal Avrami-Nakamura equation. Also, the relaxation times of both phases are function of temperature and degree of crystallization.

The second task is to generate a finite differences numerical algorithm based on the perturbation analysis proposed by Henson et al.[2] within the filament flow domain, which is here extended to the case of stress induced crystallization. In addition, the numerical scheme proposed by Ottone and Deiber[3] considering the interplay between average and local equations of the model is extended to this problem to obtain a high radial resolution of temperature, degree of crystallization and stress profiles. Consistently with experimental observations reported in the literature, the “skin-core” structure is predicted. It is relevant to indicate here that the model proposed can be evaluated from low to high take up velocities, and as the degree of crystallization becomes negligible, the one-phase model is recovered continuously.

It is then clear that this work concentrates efforts on predicting relevant phenomena of the microstructure (mainly macromolecular conformation) associated to the small radial temperature change in the filament. Thus, to be able to quantify, for instance, the skin-core generation in both phases, one must work inevitably in the 2-D domain. Having these conditions in our basic framework, we do not introduce the classical numerical approximations in the averaging process of nonlinear thermal and mechanical terms used to reduce the melt spinning model to the 1-D domain (see also a discussion on this aspect in Ottone and Deiber[3]).

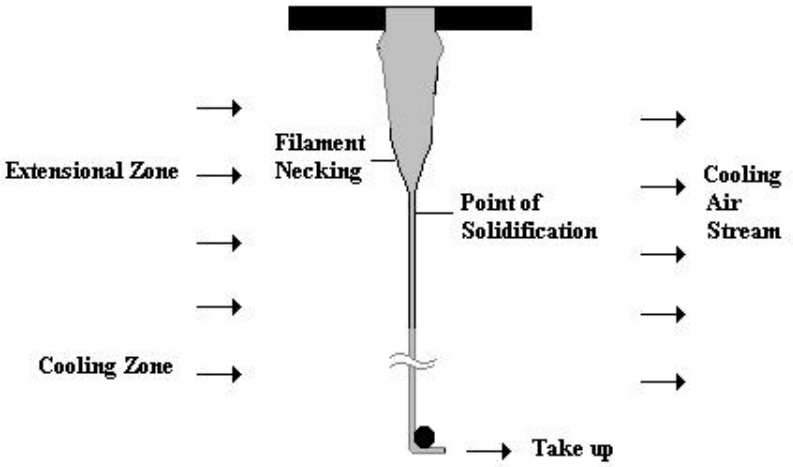


Figure 1: Scheme of the melt spinning operation involving one filament.

## 2 BASIC EQUATIONS

### 2.1 Extensional Zone

In this section we present the melt spinning model for the steady state regime in the extensional zone, which comprises the part of the filament placed from the extrusion capillary to the solidification point (the axial velocity is assumed near constant at this point; see also below). Since the polymer is considered incompressible, the mass balance implies,

$$\left(\underline{\nabla} \cdot \underline{v}\right) = 0 \tag{1}$$

where $\underline{v}$ is the velocity vector. The balance of momentum in the filament is expressed,

$$\rho\, \underline{v} \cdot \underline{\nabla} \underline{v} = -\underline{\nabla} p + \underline{\nabla} \cdot \underline{\underline{\tau}} + \rho\, \underline{g} \tag{2}$$

where $\rho$ is the polymer density, $p$ is the pressure field, $\underline{g}$ is the gravity vector and $\underline{\underline{\tau}}$ is the extra stress tensor considered symmetric throughout this work. This tensor includes the stress contributions of the amorphous $\left(\underline{\underline{\tau}}_p + \underline{\underline{\tau}}_s\right)$ and crystalline $\underline{\underline{\tau}}_c$ phases (see Eq.(14) below).

The retarded elastic response is considered in the amorphous phase through the term $\underline{\underline{t}}_s = 2h_s \underline{\underline{D}}$.[3,4]

The energy balance in the filament is,

$$\rho c_v \underline{v} \cdot \underline{\nabla} T = -\underline{\nabla} \cdot q + \underline{\underline{D}} : \underline{\underline{t}} + \rho \Delta H_f \, f_\infty \left( \underline{v} \cdot \underline{\nabla} x \right) \tag{3}$$

where $f_\infty$ is the maximum degree of crystallization of the amorphous phase assumed constant. In Eq. (3) the heat capacity is expressed as a function of temperature $T$ and degree of transformation $x$ through the following expression[1]:

$$c_v = c_s \, x f_\infty + c_1 \left(1 - x f_\infty\right) \tag{4}$$

where $c_s$ is the heat capacity of the semi-crystalline phase and $c_1$ is the heat capacity of the amorphous phase. Also, $c_s$ and $c_1$ are functions of the temperature $T$ expressed in °C, as follows:

$$c_s(T) = c_{s1} + c_{s2} T \tag{5}$$

$$c_1(T) = c_{11} + c_{12} T \tag{6}$$

The heat of fusion $\Delta H_f(T)$ is also a function of temperature[1],

$$\Delta H_f(T) = \Delta H_f(0) + \left(c_{11} - c_{s1}\right) T + \left(c_{12} - c_{s2}\right) \frac{T^2}{2} \tag{7}$$

where $\Delta H_f(0)$ is the value at the reference temperature[5]. In Eq. (3), $\underline{q} = -k_s \cdot \underline{\nabla} T$ is the heat flux vector, $k_s$ is the thermal conductivity and $\underline{\underline{D}} : \underline{\underline{t}}$ is the mechanical power. This term involves the rate of deformation tensor $\underline{\underline{D}} = \left(\underline{\nabla v} + \underline{\nabla v}^T\right)/2$ which is a function of the fluid kinematics $\underline{v}(r,z) = v_z \underline{e}_z + v_r \underline{e}_r$, where $v_z$ and $v_r$ are the axial and radial components of the velocity vector, respectively, in the cylindrical coordinate system. Here the angular component of the velocity vector is null because no perturbation in the flow field is considered.

In addition the degree of transformation $x$ is evaluated through the Avrami-Nakamura rate of crystallization, which is expressed,[1,5]

$$\underline{v} \cdot \underline{\nabla} x = m K_{av} \left(-\ln\left(1 - x\right)\right)^{(m-1)/m} \left(1 - x\right) \exp\left( z \, tr \underline{\underline{t}}_p \right) \tag{8}$$

In Eq. (8) $K_{av}$ is the Avrami kinetic parameter evaluated under null stress and $m$ is an exponent considered unity as suggested by Doufas et al.[1] Parameter $z$ is independent from temperature and determines the degree of coupling between the rate of crystallization and the stress tensor.

We use here the Phan-Thien and Tanner model (PTTM) to determine the stress $\underline{\underline{\tau}}_p$ for the amorphous phase and the rigid dumbbell for the orientation stress tensor $\underline{\underline{S}}$ of the crystalline phase immersed in the melt.

The appropriate formulation of the melt spinning model with stress induced crystallization requires the constitutive equations for the stress tensors associated to the crystalline and amorphous phases. These models are discussed below.

The viscoelastic stress $\underline{\underline{\tau}}_p$, which is a part of the amorphous stress tensor $\underline{\underline{\tau}}_a = \underline{\underline{\tau}}_p + \underline{\underline{\tau}}_s$, is expressed,

$$\underline{\underline{\tau}}_p + \lambda_a \frac{d}{dt}\underline{\underline{\tau}}_p = 2\lambda_a G \underline{\underline{D}} \tag{9}$$

for the Phan-Thien and Tanner model (PTTM).[6] In Eq. (9),

$$\frac{d}{dt}\underline{\underline{\tau}}_p = \frac{D}{Dt}\underline{\underline{\tau}}_p - \underline{\underline{L}}\cdot\underline{\underline{\tau}}_p - \underline{\underline{\tau}}_p\cdot\underline{\underline{L}}^T - \underline{\underline{\tau}}_p\frac{D\ln T}{Dt} \tag{10}$$

is the Gordon-Schowalter[7,8] non-affine time-convective derivative, where the effect of the thermal history is added through the term $D\ln T/Dt$.[3] Also $\underline{\underline{L}} = \underline{\nabla}\cdot\underline{v} - c\,\underline{\underline{D}}$ is the effective velocity gradient tensor, $\eta_p = \lambda_a G$ and $\eta_s = \eta_p(1-\alpha)/\alpha$. The instantaneous elastic response of this model can be obtained for $\alpha = 1$.[9] Here, $G$ is the relaxation modulus of the amorphous phase.

Since the melt rheological model gets the linear viscoelastic response at the asymptotic limit of small shear rates, the amorphous relaxation time can be expressed $\lambda_a(x,T) \approx \lambda_o$ with $\lambda_o = \lambda_{oo}\exp[-11.9755 + 6802/(T+273)](1-f_\infty x)^2$ as reported by Doufas and McHugh.[5] The exponential term in this expression was provided by Gregory and Watson.[10] In particular, the PTTM considers a relaxation time that is also a function of the stress tensor expressed $\lambda_a = \lambda_o / K(T, tr\underline{\underline{\tau}})$ where $K = \exp[x\, tr\underline{\underline{\tau}}/G]$, which is relevant for nonlinear responses. In this context of analysis, the relaxation modulus is also allowed to change with temperature according to $G = G_o(T/T_r)$ where $T_r$ is the reference temperature.

A rheometric characterization of this rheological model was carried out by following the same procedure described by Ottone and Deiber[4] to evaluate the rheological parameters of the PET melt with experimental data reported by Gregory and Watson[10] when $x = 0$. These data involved the shear rate flow of a sample that had the similar intrinsic viscosity as the PET used by Vassilatos et al.[11] (zero shear rate viscosity $\eta_o \approx$ 104.9 Pa s). The results obtained for the PTTM are reported in Table 1.

We consider here that the crystalline phase may be modeled as rigid dumbbells immersed in the melt, the number of which increases with the contribution of chains captured from the amorphous phase (see also references[1,5] for other situations). The conformational state of the

crystalline phase is represented by the orientation stress tensor $\underline{\underline{S}} \equiv \langle \underline{u}\underline{u} \rangle - \frac{1}{3}\underline{\underline{d}}$, where $\underline{u}$ is the unit vector along the dumbbell axis and $\underline{\underline{d}}$ is the identity tensor. Here the bracket $\langle \underline{u}\underline{u} \rangle$ in the definition of $\underline{\underline{S}}$ involves the average carried out with the conformational density distribution function of the crystalline phase. The equation giving the evolution[12] of $\underline{\underline{S}}$ for the quadratic closure approximation $\langle \underline{u}\,\underline{u}\,\underline{u}\,\underline{u} \rangle \approx \langle \underline{u}\,\underline{u} \rangle \langle \underline{u}\,\underline{u} \rangle$, is

$$\underline{\underline{S}} + l_c \frac{d}{dt} \underline{\underline{S}} = \frac{2}{3} l_c \underline{\underline{D}} - 2 l_c \left( \underline{\nabla v}^T : \underline{\underline{S}} \right) \left( \underline{\underline{S}} + \frac{1}{3}\underline{\underline{d}} \right) \tag{11}$$

where the relaxation time of the semi-crystalline phase $l_c(x,T)$ is a function of temperature and degree of transformation. Thus[1],

$$l_c(x,T) \cong c\, l_a(x,T) \exp(F f_\infty x) \tag{12}$$

In our numerical calculations, we also used the hybrid closure approximation[13] for $\langle \underline{u}\,\underline{u}\,\underline{u}\,\underline{u} \rangle$ yielding similar results. From the theory of the rigid dumbbell dynamics[12], one also shows that the stress tensor of the crystalline phase is,

$$\underline{\underline{t}}_c \cong 3 G_c \underline{\underline{S}} + \frac{G_c}{2} l_c \left( \underline{\nabla v}^T : \underline{\underline{S}} \right) \left( \underline{\underline{S}} + \frac{1}{3}\underline{\underline{d}} \right) \tag{13}$$

where $G_c$ is the corresponding relaxation modulus.

Therefore, the total extra stress tensor of the semi-crystalline phase is expressed according to the mixture theory of two phases as follows:

$$\underline{\underline{t}} = (1 - f_\infty x) \left( \underline{\underline{t}}_p + \underline{\underline{t}}_s \right) + f_\infty x \underline{\underline{t}}_c \tag{14}$$

Equation (14) is different from that proposed by Doufas et al.[1] in the sense that when $x \to 0$ the one-phase model for the low take up velocity range is recovered systematically. This asymptotic behavior is also validated through the comparison with experimental data.[3] On the other hand, for $x \to 1$ the semi-crystalline phase looses the stretching ability (system locking[1]) reaching then the solidification point at $T \approx T_s$.

In the formulation of stress tensors above, we have used the mean field approximation concerning the velocity gradient and concentration effects in Eq. (14) are neglected.[1,5]

### 2.2 Cooling Zone

After the solidification point is obtained at $T \approx T_s > T_g$, which is defined from the mechanical point of view discussed by Doufas and McHugh[5], the filament remains under heat exchange with the cooling air. This point is obtained at a temperature greater than the glassy

temperature $T_g$ of the polymer due to the increase of the crystalline phase with a high relaxation modulus. The cooling zone allows relaxations of the amorphous and crystalline phases changing the mechanical properties of the final product. Thus, in the context of the model, the filament is still under relaxation and cooling in this zone, while the velocity is approximately constant and equal to the take up velocity $v_L$. Thus, $v_z \approx v_L$ and $\frac{\partial v_z}{\partial z} \approx 0$ for $T < T_s$.

Under these kinematic and thermal conditions, the stress tensor of the amorphous phase is,

$$\underline{\underline{t}}_p + l_a \frac{d}{dt}\underline{\underline{t}}_p = 0 \tag{15}$$

for the PTTM. Also, the orientation stress tensor of the crystalline phase in this zone is,

$$\underline{\underline{S}} + l_c \frac{d}{dt}\underline{\underline{S}} = 0 \tag{16}$$

and,

$$\underline{\underline{t}}_c = 3 G_c \underline{\underline{S}} \tag{17}$$

The energy balance in the cooling zone is expressed,

$$\rho c_v \underline{v} \cdot \underline{\nabla} T = -\underline{\nabla} \cdot q + \rho \Delta H_f f_\infty \left( \underline{v} \cdot \underline{\nabla} x \right) \tag{18}$$

The last term on the right hand side of Eq. (18) is negligible because the degree of transformation is around unity. Also, the mechanical power is nearly null due to $\frac{\partial v_z}{\partial z} \approx 0$.

It should be pointed out here that the evaluation of the filament cooling for temperatures near and below the glassy temperature ($T < T_g$) requires further thermodynamic considerations associated to the phase change from a semi-crystalline melt to an elastic solid. The experimental data analyzed in this work do not cover this part of the cooling process. We designate $L_c$ the maximum filament length considered in the experimental data, and $L < L_c$ is the length from the capillary to the position where the melt reaches the solidification point at the temperature $T_s$.

## 3 BOUNDARY CONDITIONS

In this model the position $z = 0$ is placed at the outlet of the extrusion, where the boundary conditions are expressed as follows:

$$v_z = v_o, \qquad T = T_o, \qquad t_s^{zz} = t_s^{rr} = 0, \qquad S^{zz} = 0$$

$$r_o = r_c, \qquad t^{zz} = t_o^{zz}, \qquad Rel = \frac{t^{rr}}{t^{zz}}, \qquad x = 0 \tag{19}$$

where $r_o(z)$ is the fiber radius as function of the axial direction $z$, $v_o$ is the melt velocity at the capillary with radius $r_c$, and $T_o$ is the extrusion melt temperature. Also the stress ratio $Rel$ can be varied in the range $-\frac{1}{2} < Rel < 0$ for viscoelastic fluids. This result has been fully discussed in the literature,[4,14] where it was reported that numerical solutions were not sensitive for values of $Rel$ within this specific range, and that the condition $Rel \approx 0$ is a good approximation[3].

Boundary conditions involving the symmetry of fields are imposed at the centerline $r = 0$ for any position $z$. Thus,

$$\frac{\partial v_z}{\partial r} = 0, \quad \frac{\partial T}{\partial r} = 0, \frac{\partial t^{zz}}{\partial r} = 0 \quad \frac{\partial t^{rr}}{\partial r} = 0 \quad \frac{\partial S^{zz}}{\partial r} = 0, \quad \frac{\partial x}{\partial r} = 0 \tag{20}$$

while at the filament free surface for $r = r_o(z)$ and any position $z$, dynamics and kinematics constraints are,

$$\left(\underline{\underline{T}} \cdot \underline{n}\right) \cdot \underline{t} = \left(\underline{\underline{T}}_{air} \cdot \underline{n}\right) \cdot \underline{t} \tag{21}$$

$$\left(\underline{\underline{T}} \cdot \underline{n}\right) \cdot \underline{n} = -s\,\kappa \underline{n} + \left(\underline{\underline{T}}_{air} \cdot \underline{n}\right) \cdot \underline{n} \tag{22}$$

$$\underline{v} \cdot \underline{n} = 0 \tag{23}$$

$$\underline{v} \cdot \underline{t} = \underline{v}_{air} \cdot \underline{t} \tag{24}$$

for the mechanical variables, and

$$\underline{q} \cdot \underline{n} = h_e \Delta T \tag{25}$$

for the temperature field. In these equations, $\underline{n}$ and $\underline{t}$ are the unit vectors normal and tangential to the free surface, respectively, $\kappa$ is the curvature of the free surface and $s$ is the polymer-air surface tension. In addition, the total stress tensor $\underline{\underline{T}} = -p\underline{\underline{d}} + \underline{\underline{t}}$ in the filament involves the extra stress tensor $\underline{\underline{t}}$ and the pressure $p$, where $\underline{\underline{d}}$ is the unit tensor. It is assumed that $\underline{\underline{T}}_{air} \approx -p_{air}\underline{\underline{d}}$ for the cooling air. In Eq. (25), $\Delta T = T - T_{air}$ is the thermal jump between the average air temperature $T_{air}$ and the polymer temperature $T$ evaluated at the free surface

and $h_e$ is the external coefficient of heat transfer. Also, $\underline{v}_{air}$ is the velocity vector of the cooling air. Here, we are also assuming that the model for the melt spinning operation is uncoupled from the model of the cooling air, which may be an appropriate approximation when a monofilament spinning is considered[14].

Correlations required to evaluate the friction and external heat transfer coefficients are taken from Ottone and Deiber[3]. In addition, in this work we consider that the thermo-physical properties of air are function of temperature. Thus, $r_{air} \propto 1/T_{cc}$, $m_{air} \propto T_{cc}^{0.7}$ and $k_{air} \propto m_{air}$ for air density, viscosity and thermal conductivity, respectively, when values at a reference temperature $T_{air}$ are known. The value $T_{cc}$ is the arithmetic mean between the cooling air and filament temperatures.

## 4 NUMERICAL METHOD

The numerical algorithm proposed by Ottone and Deiber[3] to study the low take up velocity range has been extended here to consider the phenomenon of stress induced crystallization at high take up velocities. Thus, the balance equations associated to the description of the crystalline phase coupled to the amorphous phase described above were included in this algorithm.

It is appropriate to point out here that this iterative algorithm allows us to account for the most relevant phenomena associated to a 2-D description of temperature, degree of transformation and stress fields. With this specific target, we use the analytical coupling between the perturbed average model resulting from the rigorous radial average of the perturbed 2-D model[2,3] and the associated point-wise energy balance, rate of crystallization and constitutive equations for stresses.

The perturbed average model is solved with the Runge-Kutta method and the 2-D differential equations are solved through finite differences, which are coupled also iteratively at each axial step, where convergence criteria are imposed. The finite difference equations involve the implicit tri-diagonal algorithm for the temperature field and the explicit-implicit backward differences for the stresses and degree of transformation. Fine meshes can be generated; for instance, 100 radial nodes and axial step sizes of $10^{-5}$ m, depending these aspects on the precision required to describe the details of the filament microstructure.

It should be also pointed out here that the numerical method uses a cylindrical coordinate system $(z,r,q)$ placing the $z$-axis along the filament from the extrusion capillary to the take up roll (Figure 1). In addition, a coordinate transformation defining new variables $(Z,z,q)$ with $Z = z$ and $z = r/r_o$ is considered to achieve a 2-D rectangular computational domain.

Table 1 presents the values concerning the thermo-physical properties and rheological parameters of the PET melt as well as the model constants used in the numerical runs. Also, Table 2 indicates the processing conditions of the melt spinning operation simulated in this work. Therefore, in the section below, the numerical predictions of the model are compared with the experimental data reported by Vassilatos et al.[11]

It should be pointed out here that the numerical method also uses an outer iterative loop through a shooting method based on trial initial values of the axial stress, and it must converge to the take up velocity and solidification temperature. This numerical aspect places emphasis in that the melt spinning operation generates a two points boundary value problem (TPBVP) from the mathematical point of view (see also below).

## 5 RESULTS AND DISCUSSION

Figure 2 shows that the numerical prediction of the filament radius compares well with experimental data reported by Vassilatos et al.[11] for a take up velocity of 5490 m/min. It is also found that the appropriate friction coefficient is obtained for $b = 0.3$. From this figure it is clear that the filament necking stars when the filament radius decreases sharply to become then constant at the onset of the cooling zone, i.e. for 0.7<Z < 0.83 m, approximately. For the same situation, Figure 3 compares the numerical prediction of the average temperature profile with experimental data. It is observed here that the small plateau presented by experimental data at around $Z$=0.75 m (see also the small peak in full line described by numerical results at the same place) can be associated to the heating of the filament due to the necking phenomenon. This phenomenon increases the heat generation in the filament, which is coming from the heat of crystallization (crystallization occurs mainly in filament necking) and the mechanical power developed due to the sharp increase of stresses (see Figure 9).

In relation to the necking phenomenon, it is also relevant to analyze the evolution of the amorphous and crystalline relaxations times (see Figure 4). For instance, the crystalline relaxation time is almost null until $Z \approx 0.83$ where the cooling zone stars. The evolution of the amorphous relaxation time increases for low $Z$ to reach a maximum value, then decreases as a consequence of the sudden increment of the degree of transformation and stresses in the necking zone. Finally in the cooling zone, both relaxation times increase sharply because the filament temperature falls to low values.

Figures 5 to 7 depict the sensitivity of model responses when changes of parameters are introduced to enhance the coupling between stress and crystallization (parameter $z$ ) and filament and air (parameter $b$ ). Most of our results are similar to those reported by Doufas et al.[1] in the 1-D filament domain. These authors considered the 2-D domain for low take up velocities only.[16]

In relation to the importance of solving the melt spinning problem in the 2-D domain, Figure 8 to 11 show the 2-D calculations obtained for the temperature $T(z,Z)$ and stress difference $Dt = t_{zz}(z,Z) - t_{rr}(z,Z)$ fields, and the following microstructure variables of practical interest derived from them:

$$E_a(z,Z) = \sqrt{\frac{trt_{=a}}{3G}} \tag{26}$$

designated relative amorphous chain extension, and

$$F_c(z,Z)=\sqrt{\frac{3}{2}\underline{\underline{S}}:\underline{\underline{S}}} \tag{27}$$

which is the orientation factor. Thus, $F_c=1$ for perfect alignment and $F_c=0$ for total isotropy. In these figures one can observe that a small radial change in temperature generates the skin-core phenomenon of both the amorphous and crystalline phases. Thus $E_a(z,Z)$ and $F_c(z,Z)$ increase toward the filament-air interface after the necking is developed (black regions in Figures 10 and 11 indicating steep variations when 100 parametric lines are potted).

There are several aspects of the melt spinning model that may deserve considerations in future researches. For instance, refinements in the calculations can be introduced by modeling further the different transitions along the filament. For instance, Kannan et al.[17] have recently modeled the melt spinning operation at low take up velocities (crystallization is neglected and a 1-D filament domain is used) through a thermo-mechanical theory to be able to predict the position where the transition from melt to elastic solid initiates, having as thermodynamic data the glassy temperature. Therefore, in the shooting method only the take up velocity (the true boundary condition) must be satisfied. The results show that this zone is rather small (the initiation zone is close to the solidification point) and the associated velocity profiles are smoother than in previous calculations[4]. Nevertheless, the results also show a rather Newtonian like behavior as that found for the approximations of George.[18] One concludes here that further efforts should be placed to model the transitions zones involving $T_s$ and $T_g$ with kinematics and thermal matching conditions to get a genuine TPBVP in the high take up velocity range.

Table 1:Thermo-physical properties and rheological parameters of the PET melt.

| Parameters | Value | Reference |
|---|---|---|
| $c_{s1}$ | 0.2502 cal/gr $^oC$ | Doufas and McHugh[5] |
| $c_{s2}$ | $7\ 10^{-4}$ cal/gr $^oC^2$ | Doufas and McHugh[5] |
| $c_{11}$ | 0.4243 cal/gr $^oC$ | Doufas and McHugh[5] |
| $c_{12}$ | $5.65\ 10^{-4}$ cal/gr $^oC^2$ | Doufas and McHugh[5] |
| $DH_f(0)$ | 30 cal/gr | Doufas and McHugh[5] |
| $f_\infty$ | 0.42 | Vassilatos et al.[11] |
| $m$ | 1 | Doufas et al.[1] |
| $F$ | 5 | This work |
| $z$ | $1.3\ 10^{-6}$ | This work |
| $c$ | 0.005 | Doufas et al.[1] |
| $l_{oo}$ | 0.0125 $s^{-1}$ | Deiber and Ottone[4] |
| $G_o$ | 8400Pa | Deiber and Ottone[4] |
| $k_s$ | 0.2 W/m $^oC$ | Doufas and McHugh[5] |
| $K_{av}$ | 0.016 $s^{-1}$ | This work |
| $s$ | 0.027 Pa m | Henson el al.[2] |
| $r$ | 1200 kg/$m^3$ | Ziabicki and Kawai[15] |
| $a$ | 0.999 | This work |
| $c$ | $4\ 10^{-5}$ | Deiber and Ottone[4] |
| $x$ | $9.25\ 10^{-5}$ | Deiber and Ottone[4] |

Table 2: Processing conditions for the melt spinning operation. Experimental data are from Vassilatos et al.[11]

| Processing parameter | Value |
|---|---|
| Take up velocity, $v_L$ | 5490 m/min |
| Capillary tube radius, $r_c$ | 0.19 mm |
| Mass flow rate, $p\, r_c^2 v_o$ | 2.8 gr/min |
| Temperature at exit of capillary, $T_o$ | 310 $^oC$ |
| Initial velocity, $v_o$ | 0.302 m/s |
| Velocity of cooling air, $v_{air}$ | 0.1 m/s |
| Cooling air temperature, $T_{air}$ | 24 $^oC$ |

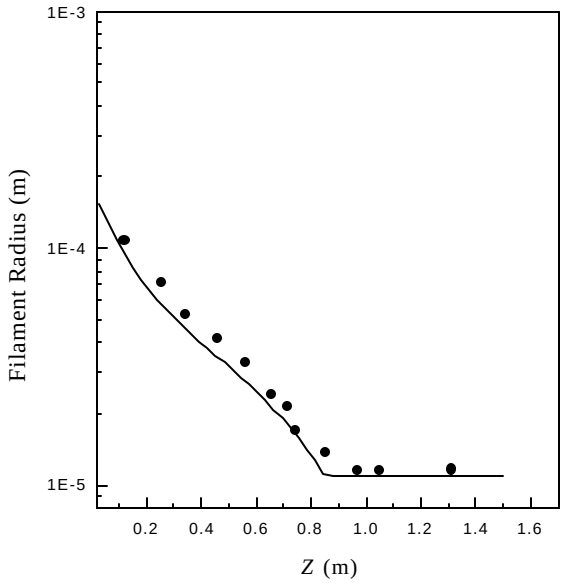


Figure 2: Numerical prediction of the filament radius along the spinline. • refers to experimental data of Vassilatos et al.[11] for a take up velocity of 5490 m/min, $T_s = 165$ °C and $b = 0.3$.

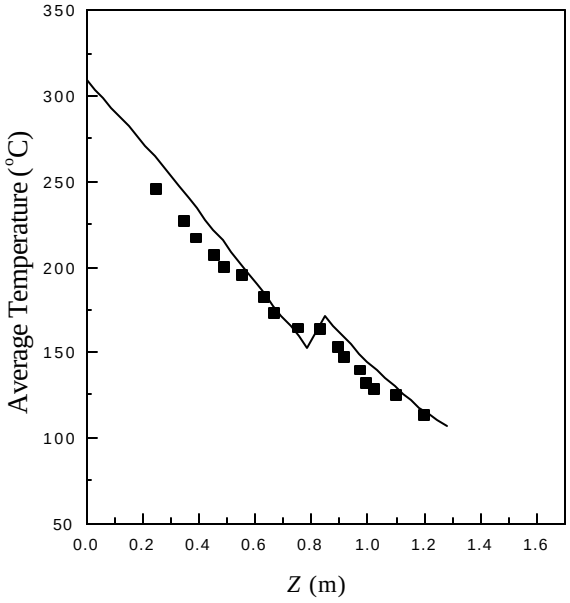


Figure 3: Numerical prediction of the average temperature profile along the spinline. ■ refers to experimental data of Vassilatos et al.[11] for a take up velocity of 5490 m/min, $T_s = 165$ °C and $b = 0.3$.

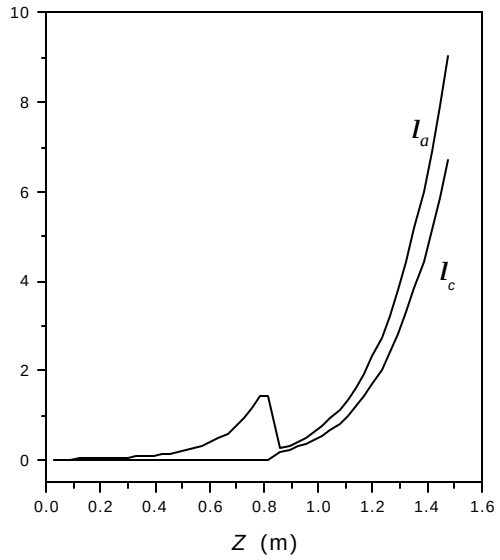


Figure 4: Numerical predictions of amorphous and crystalline relaxation times for a take up velocity of 5490 m/min, $T_s = 165$ °C and $b = 0.3$.

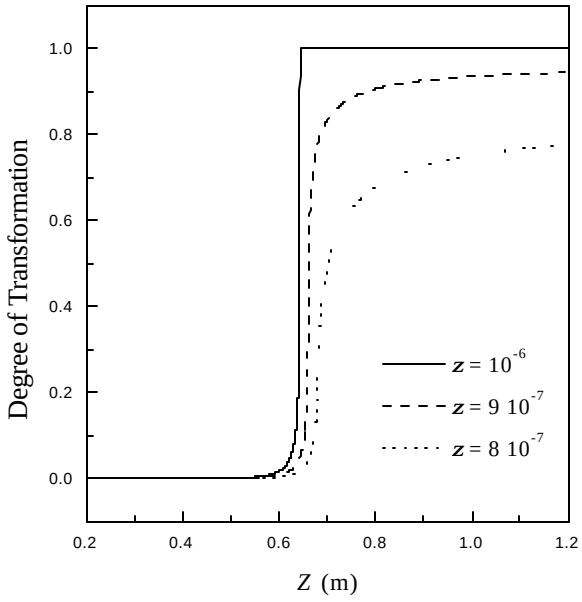


Figure 5: Numerical predictions of the effect of parameter $z$ on the degree of transformation. Input parameters and processing conditions are included in Tables 1 and 2. Also, $T_s = 180$ °C and $b = 0.33$.

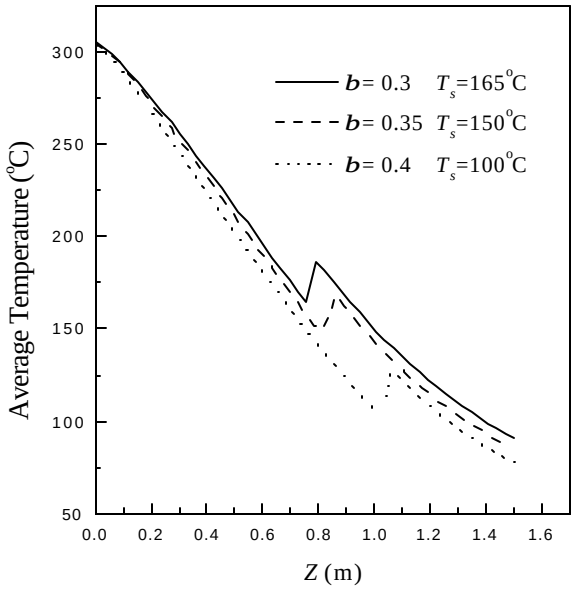


Figure 6: Numerical predictions of the effect of parameter $b$ on the average temperature profile. Input parameters and processing conditions are included in Tables 1 and 2.

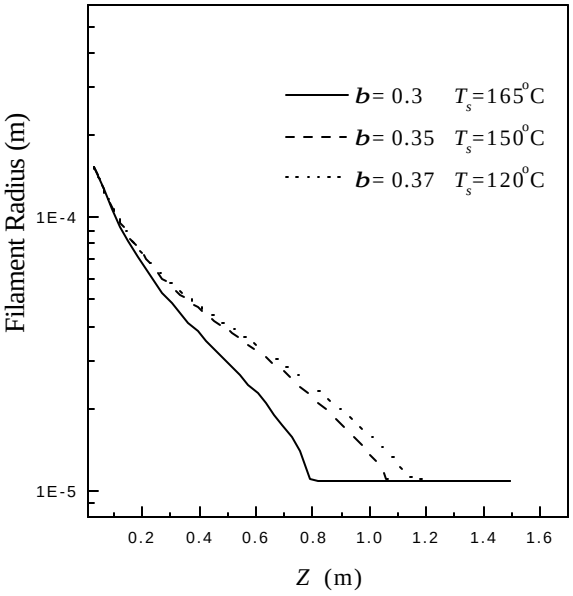


Figure 7: Numerical predictions of the effect of parameter $b$ on the filament radius. Input parameters and processing conditions are included in Tables 1 and 2.

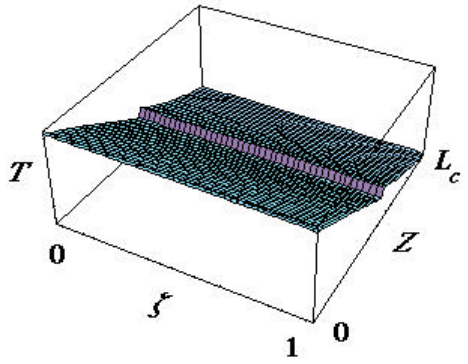


Figure 8: Numerical prediction of the temperature field $T(z, Z)$ for the experimental situation of Vassilatos et al.[11] at a take up velocity of 5490 m/min.

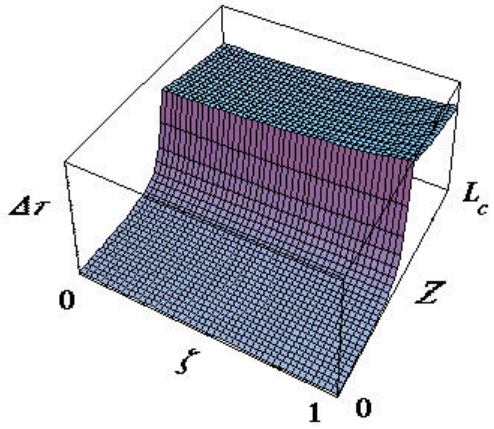


Figure 9: Numerical prediction of the stress difference field $Dt = t_{zz}(z, Z) - t_{rr}(z, Z)$ for the experimental situation of Vassilatos et al.[11] at a take up velocity of 5490 m/min. The maximum value is $10^7$ Pa.

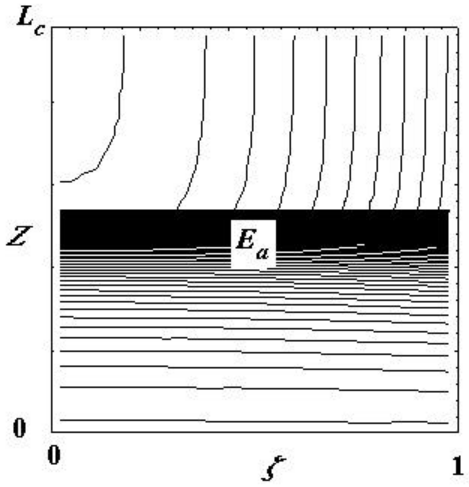


Figure 10: Numerical prediction of the relative amorphous chain extension field $E_a(\zeta, Z)$ for the experimental situation of Vassilatos et al.[11] at a take up velocity of 5490 m/min. The maximum value is 34 at $Z = L_c$.

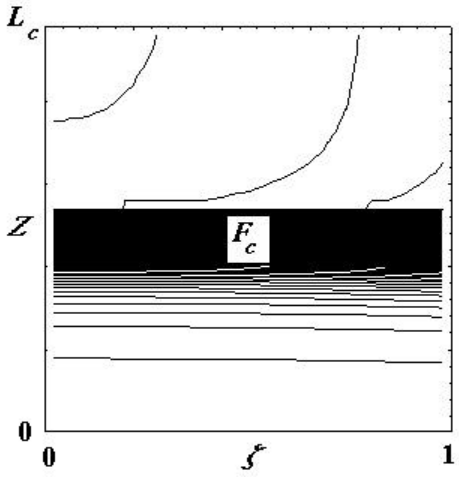


Figure 11: Numerical prediction of the orientation factor field $F_a(\zeta, Z)$ for the experimental situation of Vassilatos et al.[11] at a take up velocity of 5490 m/min. The maximum value is 0.92 at $Z = L_c$ and the minimum is $6\ 10^{-4}$ at $Z = 0$.

## 6 CONCLUSIONS

More precise calculations than those reported previously with 1-D models are required in the modeling of melt fiber spinning at high take up velocities in order to explore details of the filament microstructure.. For this purpose, the perturbed 2-D model described in this work must be solved. A numerical algorithm based on finite differences that allows one to obtain precise radial resolution of temperature, degree of transformation and stress fields is proposed here. It is also shown that the rheology of the filament can be approximately described through a constitutive equation that results from the combination of the Phan-Thien and Tanner viscoelastic model for the amorphous phase and the kinetic model of the rigid dumbbell for the crystalline phase immersed in the melt. Numerical predictions of the model compare well with experimental data published in the literature. Also, the developments of skin-core structures of crystalline and amorphous phases are obtained.

## 7 ACKNOWLEDGMENTS

*The authors are thankful for financial aid received from the CONICET (Consejo Nacional de Investigaciones Científicas y Técnicas, Argentina) PIP 4811/97 and the Secretaría de Ciencia y Técnica de la UNL (Universidad Nacional del Litoral, Argentina) Programación CAI+D 96.*

## 8 REFERENCES

[1] A. K. Doufas, A. J. McHugh and Ch. Miller, "Simulation of Melt Spinning Including Flow-Induced Crystallization. Part I. Model Development and Predictions", *J. Non-Newtonian Fluid Mech.*, **92**, 27-66 (2000).

[2] G.M. Henson, D. Cao, S.E. Bechtel and M.G. Forest, "Thin-filament melt spinning model with radial resolution of temperature and stress", *J. Rheol.*, **42**, 329- 360 (1998).

[3] M.L. Ottone and J.A. Deiber, "A numerical method for the viscoelastic melt spinning model with radial resolutions of temperature and stress field", *Industrial & Engineering Chemistry Research*, in press (2002).

[4] M.L. Ottone and J.A. Deiber, "Modeling the melt spinning of polyethylene terephthalate", *J. Elast. Plast.*, **32,** 119-139 (2000).

[5] A.K. Doufas and A.J. McHugh, "A. Simulation of Melt Spinning Including Flow-Induced Crystallization. Part III. Quantitative Comparisons with PET Spinline Data", *J. Rheol.*, **45**, 403-420 (2001).

[7] R.G. Larson, *Constitutive equations for polymer melts and solutions*, Butterworths Series in Chemical Engineering; Butterworth Publishers (1988).

[6] F. Sugeng, N. Phan-Thien and R.I. Tanner, "A study of non-isothermal non-newtonian extrudate swell by a mixed boundary element and finite element method", *J. Rheol.*, **31**, 37-58 (1987).

[8] R.J. Gordon and W.R. Schowalter, "Anisotropic fluid theory: a different approached to the dumbbell theory of dilute polymer solutions", *Trans. Soc. Rheol.*, **16**, 79-97 (1972).

[9] M.M. Denn, "Issues in Viscoelastic Flow",. *Ann. Rev. Fluid Mech.*, **22**, 13-34 (1990).

[10] D.R. Gregory and M.T. Watson, "Steady state properties of poly(ethylene terephthalate) melts", *J. Polym. Sci*., **30**, 399-406 (1970).
[11] G. Vassilatos, B.H. Knox and H.R.E. Franfort, "Dynamics, structure development and fiber properties in high speed spinning of polyethylene terephthalate", in *High-Speed Fiber Spinning*; Eds. A. Ziabicki and H. Kawai, John Wiley & Sons: New York, (1985).
[12] R.B. Bird, O. Hassager, R.C. Armstrong and Ch.F. Curtiss, "Dynamics of Polymeric Liquids. Kinetic Theory", Vol. II, John Wiley & Sons, New York (1977).
[13] S.G. Advani and C.L. Tucker, "the use of tensors to describe and predict fiber orientation in short fiber composites", *J. Rheol.*, **31**, 751-784 (1987).
[14] M.M. Denn, *Computational analysis of polymer processing*; Pearson, J. R. A., Richardson, S. M. Eds.; Applied Science Publishers: New York, (1983).
[15] A. Ziabicki and H. Kawai, *High-Speed Fiber Spinning*; John Wiley & Sons: New York, (1985).
[16] A.K. Doufas and A.J. McHugh, "Two-dimensional simulation of melt spinning with a microstructural model for flow-induced crystallization", *J. Rheol*., **45**, 855-879 (2001).
[17] K. Kannan, F.J. Rao, and K.R. Rajagopal, " A thermo-mechanical framework for the glass transition phenomenon in certain polymers and its application to fiber spinning", *J. Rheol*., **46**, 977-999 (2002).
[18] H.H. George, "Model of steady-state melt spinning at intermediate take-up speeds", *Polym. Eng. Sci*., **22**, 292-299 (1982).